Received: 14 January 2020 | Revised: 25 March 2020 | Accepted: 25 March 2020

DOI: 10.1002/er.5459

RESEARCH ARTICLE

INTERNATIONAL JOURNAL OF ENERGY RESEARCH WILEY

The study of optimal parameters of oxygen-enriched combustion in fluidized bed with optimal torrefied woody waste

Yueh-Heng Li | **Wei-Chieh Kuo**

Department of Aeronautics and Astronautics, National Cheng Kung University, Tainan, Taiwan

Correspondence
Yueh-Heng Li Affiliation: Department of Aeronautics and Astronautics, National Cheng Kung University, Tainan 701, Taiwan.
Email: yueheng@mail.ncku.edu.tw

Funding information
Ministry of Science and Technology, Taiwan, Grant/Award Numbers: MOST 106-2923-E-006-003-MY3, MOST 106-3113-E-006-002-CC2, MOST 108-2628-E-006-008-MY3

Summary

The study explored the oxygen-enriched combustion behavior of torrefied waste wood pellets in a fluidized bed. For biomass torrefaction, three indexes, namely energy yield index (EY), proximate analysis-based index (PA), and effective comprehensive combustion index (S_{mix}), are used to present the optimal conditions from each viewpoint. Four operating parameters, incorporating torrefaction temperature, residence time and nitrogen flow rate, were taken into consideration in this study. The signal-to-noise ratios of each parameter were evaluated to examine the influencing impact of different factors. The optimal results were employed in the investigation of biochar combustion using a laboratory-scale fluidized-bed reactor with oxygen lancing. Oxygen was injected into different zones of the fluidized bed to investigate its influence on combustion efficiency. The parameters of biochar combustion optimization include torrefied materials, fluidized-bed temperature, oxygen inlet position, and oxygen concentration. The total fluidized-bed efficiency and the volatile combustion ratio were evaluated.

KEYWORDS

biochar, fluidized bed, oxygen-enriched combustion, Taguchi method, Torrefaction

1 | INTRODUCTION

Waste-to-energy generation equipment is used to process general or industrial waste into fuels to directly reduce pollution, increase the calorific value of raw materials, and convert them into electricity with an overall efficiency of more than 25%.[1] The advantages of using waste-to-energy equipment include decreased quantity of waste, superior control of odor and noise, incorporation of heat and energy produced,[2] and prevention of methane gas production in landfills. However, commissioning an incineration plant is expensive, and incinerators produce smoke during the burning process, smoke which includes acidic gases, carcinogenic dioxins, particulates, heavy metals, and nitrogen oxide. Given the versatile composition of municipal solid waste (MSW), incinerating MSW in a conventional furnace or incinerator may not prevent contamination and clogging.[3,4] Consequently, a tailored burning process and incineration facility are required as well as an in situ monitoring and control system to comply with emissions restrictions.

In recent years, oxygen-enriched combustion, among other methods, has been used to improve combustion conditions.[5] Wang et al demonstrated that the combustion area becomes more concentrated and the temperature inside the combustion chamber increases while the initial oxygen concentration raises.[6] Wall et al stated that high percentages of CO_2 and H_2O in combustion gases can increase gas emissivity and reduce the volume of flue gas from a power plant by 80%.[7] Moreover, a high oxygen concentration in the carrier gas reduces CO emission, and as the O_2 concentration increases, the total combustion efficiency increases.[8] However, Luo et al found that the effect of improvement in combustion activities diminishes at oxygen concentrations exceeding 40%.[9] Kayahan et al found that at oxygen concentrations between 21% and 30%, NO and SO_2 emissions increase owing to oxygen enrichment.[10] Although pure oxygen combustion can be employed in a limited number of fields, the adoption of oxygen-enriched combustion lowers the threshold of use conditions, reduces the volume of exhaust gases, and weakens the heat transfer effect.[11] By directly lancing oxygen into the combustion chamber, burnout without NO formation can be improved.[12] Li et al[13,14] designed a single-pellet combustion chamber to assess the combustion characteristics of coal pellets blended with biochar. Corna and Bertulessi indicated that with the appropriate selection of the oxygen lancing area, this method can improve unit operation and reduce CO emissions.[15]

The most ordinary genres of biomass combustion systems are fixed-bed and fluidized-bed combustion systems.[16,17] A fixed bed reactor, also called a packed-bed reactor, is a reactor packed with a solid catalyst or solid reactant to affect a heterogeneous reaction. The solid matter is usually composed of particles of sizes 2 to 15 mm that are deposited into a bed of a certain height (or thickness). The variety of particle sizes means that a wide range of fuel properties are available and fewer preparatory measures are required for fixed-bed combustion.[18] Furthermore, the particles in the bed (such as sand) are affected by upward airflow, and when the flow reaches a certain speed, the particles are suspended in it. This condition is called the lowest fluidization velocity, which varies with particle size and bed depth.[19] The bed of turbulent solid particles is fluidized to resemble a boiling liquid in appearance and behavior. Because of the liquid-like behavior of the fluidized bed, it is easy to control the bed interface and temperature. The solid fuel enters the splash zone of the furnace at a velocity slightly higher than the fluidization velocity, and the ascending airflow and combustion gases emanate from the splash zone. Strenuous movement of the bed allows the fuel to mix quickly, be adsorbed by the hot bed material (sand, ash, and fuel), and rapidly release fuel moisture and volatiles, which raises the temperature to the point of ignition. A relatively large amount of pulsating bed material continuously exposes new surfaces of the fuel particles, maintaining rapid combustion within the bed, which results in good load response.[20] The advantages of fluidized-bed combustion include clean combustion with a desulfurization rate higher than that of other combustors,[21] reduced NO_x emissions,[22] fuel adaptability, especially for medium- and low-sulfur fuels, and high combustion efficiency of up to 95% to 99%.[23] Nonetheless, some challenges evoke from the fluidized-bed combustion, such as fuel segregation,[24] bed agglomeration,[25] and volatile escape from the lower dense bed.[26]

Biomass is regarded as the worldwide and most general renewable energy, and approximate 2.8 billion people use biomass for cooking according to the report of Energy Access Outlook 2017. However, owing to its low heating value (HV), direct burning of biomass results in poor combustion efficiency. Owing to increased levels of environmental awareness worldwide and the worsening of global warming, effective usage of biomass instead of fossil fuels to reduce carbon dioxide emissions is among the most important energy-related challenges facing humanity. The replacement of fossil fuels with biomass in the form of torrefied municipal waste does have a few advantages. Biomass, similar to any other fuel, will emit certain pollutants, such as CO_2, NO_x, and SO_x, when it is burned.[27] With oxygen-enriched combustion, the combustion efficiency of biomass could be increased in a remunerative approach.

The present study applied oxygen-enriched combustion to MSW in a fluidized bed. The study entailed two parts. The first was basic research on waste treatment, using the Taguchi method to find the optimal heat-treatment conditions under different combustion indexes.[4] The generated biochar was subjected to physicochemical analysis to design a fluidized-bed combustion experiment for reference. The second part was a study of the combustion characteristics observed in the fluidized-bed combustion experiment. To this end, a laboratory-scale fluidized bed was designed. Raw materials with different torrefaction levels were subjected to a batch-combustion test to observe their combustion characteristics and pollutant emissions as well as to optimize the operating parameters.

2 | EXPERIMENTAL APPARATUS AND METHODS

2.1 | Biomass materials

At present, Taipei, Taichung City, and Tainan City are home to more than 80 000, 120 000, and 300 000 alee trees, respectively. The various genera include *Koelreuteria*, *Ceiba*, and *Eucalyptus*—all hardwood trees. Regular trimming is an important part of the maintenance routine of these alee trees. The advantages of trimming include improved public safety, management of tree health, the formation of good mechanical structure of trees, and correction of tree defects. This process, however, produces large amounts of waste wood that can be used for other purposes.

In this study, we shaped a mix of waste wood from all types of hardwood alee trees into pellets, each weighing approximately 1 g, with a diameter of 7 mm, and length of 10 mm, as shown in Figure 1A. All materials were sun-dried for 7 days and wood pellets were not easily blown away due to its bulk volume. A rotary miller was used to grind the pellets into particles of sizes 0.425 to 0.88 mm. A photograph of the pulverized pellets is shown in Figure 1B. Regarding element analysis, alee trees consist of 44.3% of C, 5.9% of H, and 49.1% of O. Proximate analysis was employed to determine the percentages of moisture (M), volatile matter (VM), fixed carbon (FC), and ash (ASH). ASH is the inorganic solid residue after complete burnout, incorporating calcium, iron, aluminum and silica.[28] Additionally, trace amounts of potassium, sodium, magnesium, and titanium could be found in the residue. Raw alee tree material contains 3.3% M, 87% VM, 6.9% FC, and 2.3% ASH. The high heating value (HHV) of the raw material is 18 410 MJ/kg (4400 kcal/kg).

2.2 | Experimental apparatus and measurement system

The biomass was placed in a tubular furnace to conduct torrefaction experiments. The tubular furnace was built in house, consisting of an electric furnace, large quartz tube, small quartz chamber, vacuum pump, and filter. A schematic of the torrefaction system is presented in Figure 2.

A large quartz tube with a diameter of 45 mm and a length of 350 mm encompassed the electric heater. This quartz tube was employed as the carrier gas channel to separate the heating area (heating tube). A smaller quartz tube with a stainless steel cap was placed inside the large tube and inserted into the heater. This small quartz tube with a diameter of 15 mm was the reaction chamber in which the raw materials were set and heated (reaction tube). Holes with a diameter of 1.2 mm were punched equidistantly on both sides of the cap to allow passage of the carrier gas to react with the biomass materials. A vacuum pump and pressure gauge were connected downstream of the reaction zone to evacuate air from the chamber. Exhaust gas and liquids were routed to pass through a cooling tank maintained at a constant temperature of 10°C to reduce the temperature of the flue gas. The condensable part was collected with a U-tube, and the noncondensable part was passed through an activated carbon filter to purify the gas emission.

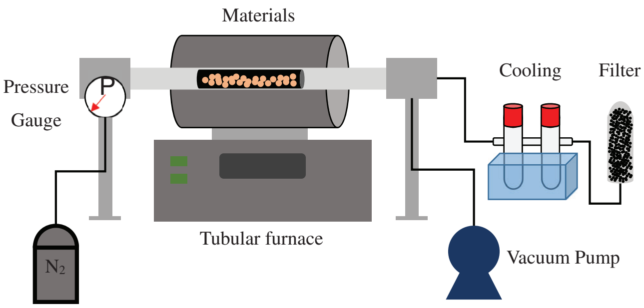

FIGURE 2 Schematic of the torrefaction system [Colour figure can be viewed at wileyonlinelibrary.com]

For each experiment, approximately 15 g of raw pulverized biomass was distributed evenly in the reaction tube. In general, one-third of the reaction tube was filled with the biomass material. After screwing the cap onto the reaction tube, the reaction tube was placed inside the heating tube. The reaction tube must be inserted inside the electric heater to ensure that all of the biomass is heated uniformly and to the proper temperature. To this end, the vacuum pump was employed to evacuate air from the heating tube and ensure that the entire environment was airtight. This step was very important for this experiment because the presence of oxygen would have led to the combustion of the biomass rather than

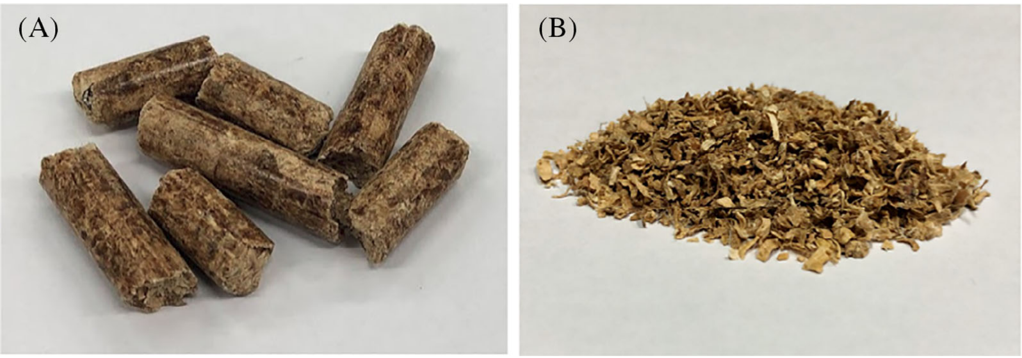

FIGURE 1 Photo of raw biomass: A, alee tree pellets; B, pulverized alee tree pellets [Colour figure can be viewed at wileyonlinelibrary.com]

torrefaction. After ensuring that the entire equipment was sealed, N_2 was introduced into the heating tube as the carrier gas in the torrefaction experiment. The N_2 flow rate was controlled with a rotameter. In addition, an electric heater with a proportional-integral-derivative (PID) controller was employed to govern the torrefaction temperature.

Thermogravimetric analysis (TGA) is performed to detect weight changes in a material as a function of temperature or time. Thermogravimetric measurements provide information with regard to the physical and chemical properties of materials[29]; for example, chemisorption, devolatilization, decomposition, and solid-gas phase reactions (such as oxidation or reduction). A PerkinElmer STA8000 was used for TGA measurement in this study. The sensitivity of the scale was 0.1 μg, and the maximum heating range was 1500°C. The PerkinElmer STA 8000 features with precise temperature and gas control, a balance with microgram sensitivity, and software to expedite and automate the analysis. The sample crucible and the empty reference crucible were placed in two separate but similar electric heating furnaces. The two furnaces must be heated or cooled linearly at any time. When the samples absorb or release heat, the temperature difference between the sample crucible and reference crucible increases, at which point the TGA computer system adjusts the electric power input to maintain both sides of the balance in isothermal equilibrium. A temperature graph was plotted in accordance with the current value of power consumed. A differential scanning calorimetry heat flow graph illustrating the heat released or absorbed by the sample during the chemical reaction was plotted. For a single experiment, approximately 7 to 10 mg of ground material (particle size <0.075 mm) was consumed. In addition, TGA enables to conduct combustion experiments, where the materials were heated from 30 to 1030°C at a heating rate of 20°C/min in an air environment.

A calorimeter is used to measure the calorific value of a material. It can be used to measure chemical reactions and thermal changes in physical processes or to determine the heat capacity of a material. A Parr 6200 series calorimeter was employed to gauge the HVs of distinct torrefied biochar samples. First, a certain quantity of substance (approximately 1 g) was placed in the crucible. Then, the crucible was placed in a stainless steel bomb, filled with O_2, and sealed thoroughly. Thereafter, the stainless steel cylinder was placed in a well-insulated sink filled with 2 L of water, and the substance was ignited after 15 seconds. By measuring the increase in the temperature of the calorimeter and of the water inside the sink, the total heat released by the substance upon combustion can be computed. Because some moisture condenses in the inner part of the stainless steel sleeve, the obtained HV is the high HV (HHV).

A laboratory-scale fluidized-bed combustor was designed and fabricated. The fluidized bed consisted of three parts: upper and lower stainless steel caps and a 1000-mm long stainless steel pipe. A schematic of this combustor is shown in Figure 3. The inner diameter was 50 mm uniformly. The carrier gas was delivered through a 2-inch. hole on the lower cap. This carrier gas was made to pass through a 400-mm long rectification zone, 50-mm long silica sand bed zone, and 550-mm long freeboard zone. Thereafter, the flue gas left the fluidized bed through a 2-inch hole on the upper cap. The flue gas was then channeled into two washing bottles filled with water for preliminary filtration, after which it was passed through activated carbon for deodorization and secondary filtration. A U-tube stuffed with cotton was placed at the end to ensure that no particles or solid unburnt carbon remained in the flue gas. Clean flue gas was pumped into the Vario Plus Industrial gas analyzer (MRU Instruments Inc.) for evaluation of its composition in terms of CO, CO_2, NO_x, and unburnt hydrocarbon (equivalent to CH_4 content).

Four *k*-type thermocouples measuring 4.8 mm in diameter and 55 mm in length of the fluidized-bed combustor were used to surveil the temperature distribution inside the fluidized bed. From the bottom, the first thermocouple was located at 385 mm, below the air distribution board and silica sand bed but above the rectifier section. The temperature detected by this thermocouple would not be affected by the combustion in the bed zone, but it still represents the temperature of the bed zone. The purpose of this thermocouple was to provide feedback to the PID controller of the electric power supply used to control the heat flux output. The second thermocouple was inserted at 420 mm, at the center of the silica sand bed zone, and it was employed to track the bed temperature in real time. The third thermocouple was attached at 590 mm, at the center of the freeboard area, in which the flame appears. However, owing to flame instability, the temperature measured by this thermocouple was not stable either. The last thermocouple was located at 900 mm, and it was used to measure the flue gas temperature.

To investigate the effect of oxygen lancing on biomass combustion, two holes measuring 3 mm in diameter were drilled on the side of the fluidized bed. The first hole was located at 450 mm, just above the bed zone. The second hole was located at 550 mm, at the center of the freeboard zone, in which the flame burns. Two 1500 W ring heaters were assembled with the fluidized-bed reactor to heat the carrier gas and silica bed to their designated temperatures. With a diameter of 55 mm and a height of

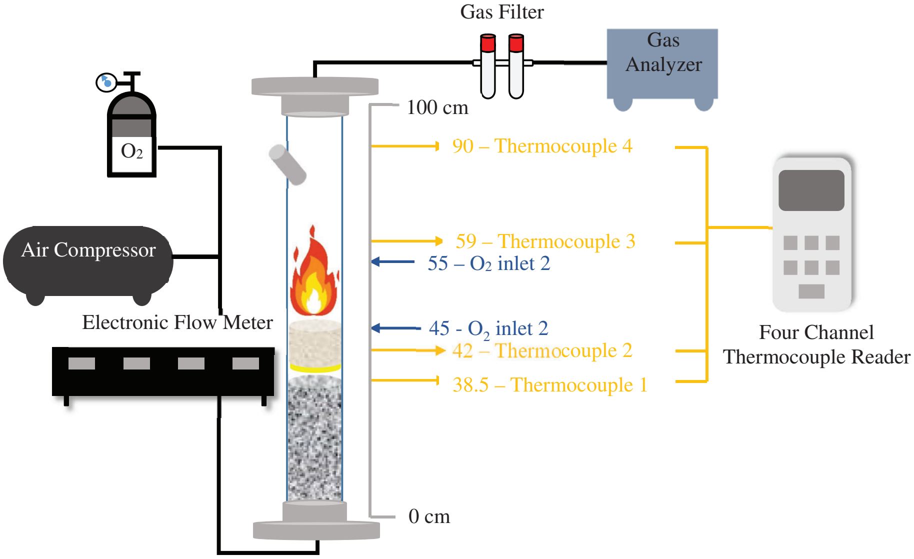

FIGURE 3 Schematic of lab-scale fluidized-bed combustor [Colour figure can be viewed at wileyonlinelibrary.com]

200 mm, the two heaters encompassed both the rectifier section and the bed section. The electric heater was powered with a 220 V power supply with a maximum current of 20 A. The maximum temperature of 850°C was recorded in the bed zone. The entire fluidized bed was shielded with 30-mm thick high-temperature cotton insulation to diminish heat loss from the bed walls and maintain the bed temperature. It is noted that the measurement uncertainty of all equipment used in this study is less than 5%.

2.3 | Optimization method

The Taguchi method was proposed by Dr. Taguchi Yuichi in the 1950s. The method employs a common orthogonal table experimental design and simple art analysis.[30] By applying the Taguchi method to a small amount of experimental data, one can significantly meliorate product quality. Finding the objective function that best expresses the quality characteristics is the core of optimization. Taguchi defined quality as the total cost of the product in its lifecycle, which is called quality loss. The smaller the quality loss, the higher the product quality is. The quality characteristic is measured using the quality loss function of a quadratic curve. When the quality characteristic fully meets the target value m, the quality loss is 0; when the quality characteristic deviates from the target value m, the quality loss increases with the speed of the quadratic curve. If there are n products, the total quality loss is

$$\text{Total quality loss} = \sum_{i=1}^{n} k(y_i - m)^2, \tag{1}$$

where y_i is the actual value, and k is a quality loss constant.

The average quality loss (Q) can be written as

$$Q = \mathrm{k}\frac{\sum_{i=1}^{n}(y_i - m)^2}{n} = k\left[(\bar{y} - m)^2 + \sigma^2\right], \tag{2}$$

where σ^2 denotes the variance of the actual value, and $\bar{y}$ denotes the average actual value.

The quality characteristic can be categorized into one of three forms: larger-the-better, smaller-the-better, and nominal-the-best. For larger-the-better, the quality characteristic is usually the desired output; for example, the HV of torrefied biochar. For smaller-the-better, the quality characteristic is usually an unwanted output; for example, unwanted byproducts or side effects. For nominal-the-best, the quality characteristic is usually a nominal output, such as a ratio of chemicals or mixtures.

An orthogonal array is presented as $L_a(b^c \times d^e)$, which means that in total, there are "a" group of experiments that accommodate up to $\boldsymbol{c}$ levels of $\boldsymbol{b}$ factors and $\boldsymbol{e}$ levels of $\boldsymbol{d}$ factors. L is taken from Latin square. Taking $\mathrm{L}_{18}(2^1 \times 3^7)$ as an example, the experimental matrix comprises one factor (F1) with two levels and seven factors (F2-F8) with three levels. With all the factors and levels, the entire experiment includes $2^1 \times 3^7 = 4373$ experiment sets. It is not feasible to search for and fulfill the optimal condition with an enormous number of experiments. With the Taguchi method, the experiment can be shrunk to 18 experiment sets, which are Exp. 1 to 18 in Table 1, but one can still explore the effects of all factors. Take experiment No. 7 as an example.

TABLE 1 L_{18} orthogonal array

Exp.\Factor	F1	F2	F3	F4	F5	F6	F7	F8
1	1	1	1	1	1	1	1	1
2	1	1	2	2	2	2	2	2
3	1	1	3	3	3	3	3	3
4	1	2	1	1	2	2	3	3
5	1	2	2	2	3	3	1	1
6	1	2	3	3	1	1	2	2
7	1	3	1	2	1	3	2	3
8	1	3	2	3	2	1	3	1
9	1	3	3	1	3	2	1	2
10	2	1	1	3	3	2	2	1
11	2	1	2	1	1	3	3	2
12	2	1	3	2	2	1	1	3
13	2	2	1	2	3	1	3	2
14	2	2	2	3	1	2	1	3
15	2	2	3	1	2	3	2	1
16	2	3	1	3	2	3	1	2
17	2	3	2	1	3	1	2	3
18	2	3	3	2	1	2	3	1

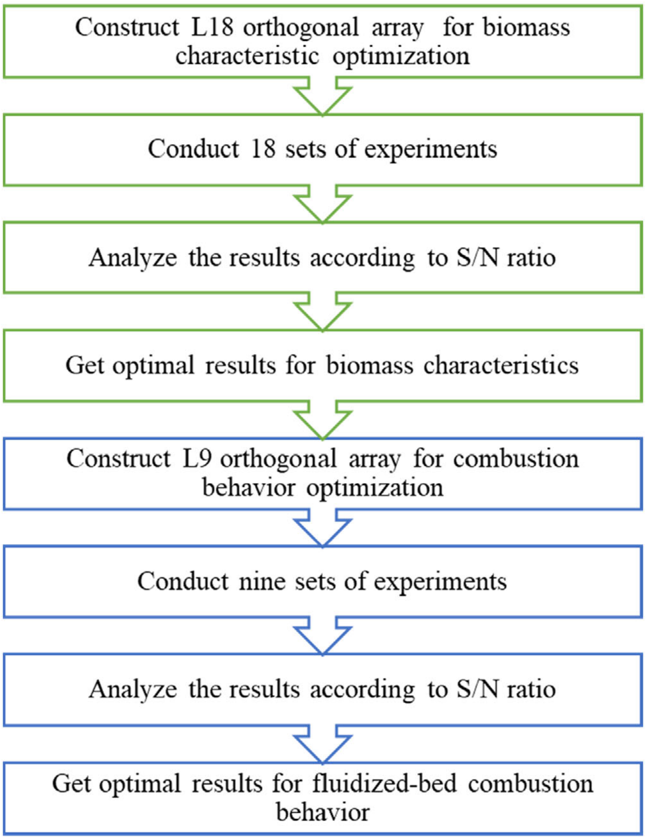

FIGURE 4 Experimental flow diagram [Colour figure can be viewed at wileyonlinelibrary.com]

2.4 | Experimental procedure

The primary objective of this research was to explore the combustion characteristics of a fluidized bed under different optimal torrefaction conditions and bed temperatures and the oxygen lancing technique under oxygen-enriched conditions. The entire study can be divided into two parts, namely biomass characteristic optimization and fluidized-bed combustion behavior optimization. In the flow diagram in Figure 4, the green and blue parts denote the biomass characteristic optimization part and the fluidized-bed combustion behavior optimization part, respectively. The procedure of the first part started with the construction of an orthogonal array (18 sets of experiments) for investigating biomass torrefaction. After completion of the 18 experiments, the results were analyzed in terms of the signal-to-noise (S/N) ratio to obtain the optimal results. We used the results obtained from the previous optimization procedure in the second part of the experiment to investigate another factor. In the second part of the experiment, we constructed an orthogonal array according to the selected factor and level. An L9 orthogonal array was constructed, and nine sets of experiments were created. After completion of these experiments, we calculated the S/N ratio of each experiment to obtain the optimal combustion behaviors. The study outcomes provide advice for industrial use or in further studies on biomass combustion.

3 | OPTIMIZATION OF BIOMASS CHARACTERISTIC

3.1 | Index selection

To optimize the biomass characteristic after torrefaction, the accuracy and reliability of the optimization are contingent on the proper selection of the optimal index in the Taguchi method. Many aspects of combustion can be considered. For example, fuels with high HVs release large amounts of heat, high FC content in biofuels prolong combustion time, and the presence of a high proportion of VM in a biofuel reduces ignition temperature. By choosing a combined index in the Taguchi method rather than a simple index, one can explore a greater number of aspects of combustion. In this study, three aspects of combustion were considered in the optimization, namely energy stored in biochar, material analysis of biochar, and the combustion feature of biochar.

3.1.1 | Energy yield

Energy yield (EY) refers to the total energy obtained from harvesting an energy source. It is the fraction of the original energy in the biomass remained after thermal degradation, such as torrefaction. To determine the EY, both the weight and the HV of the biomass before and after torrefaction were considered. The variation trends in weight and HV were different. With a higher degree of torrefaction, the weight of the final biochar would be low but HV would be high. Both phenomena are important and must be considered, so we included the EY in the Taguchi method. Consequently, the total energy stored in the biomass before and after torrefaction was required. The energy stored in the biomass can be determined as the product of mass and the HV of the product. EY can then be expressed as

$$\mathrm{EY} = \frac{\text{mass of product} \times \text{HV of product}}{\text{mass of biomass feed} \times \text{HV of biomass feed}} \times 100\%. \tag{3}$$

3.1.2 | Effective comprehensive combustion index

In solid fuel combustion, two major factors, namely ignition feature and burning performance, are vital for outlining the combustion characteristics and efficiencies.[31,32] The comprehensive combustion characteristic index (S index) was used to provide a straightforward method for assessing solid fuel combustion.[14] This index considers ignition temperature, burnout temperature, mean weight loss rate, and maximum weight loss rate. A high value of the S index indicates a better combustion reaction.[33] The S index is expressed as follows:

$$\mathrm{S} = \frac{\left(\frac{dW}{d\tau}\right)_{\max} \cdot \left(\frac{dW}{d\tau}\right)_{\text{mean}}}{{T_i}^2 \times T_b}, \tag{4}$$

where $\left(\frac{dW}{d\tau}\right)_{\max}$ is the maximum weight loss rate, $\left(\frac{dW}{d\tau}\right)_{\text{mean}}$ the average weight loss rate, T_i the ignition temperature, and T_b the burnout temperature.

Blue lines in Figure 5 denote the curves of TG, and meanwhile green lines denote the curves of differential thermogravimetric (DTG). Under the circumstances of oxidation, T_i was obtained using the cross method.[14] As shown in Figure 5A, auxiliary lines extend from the two points on the weight loss curve, namely the end of moisture evaporation and the maximum weight loss. T_b denotes the burnout temperature when the fuel conversion rate (α) reached 99%.[34]

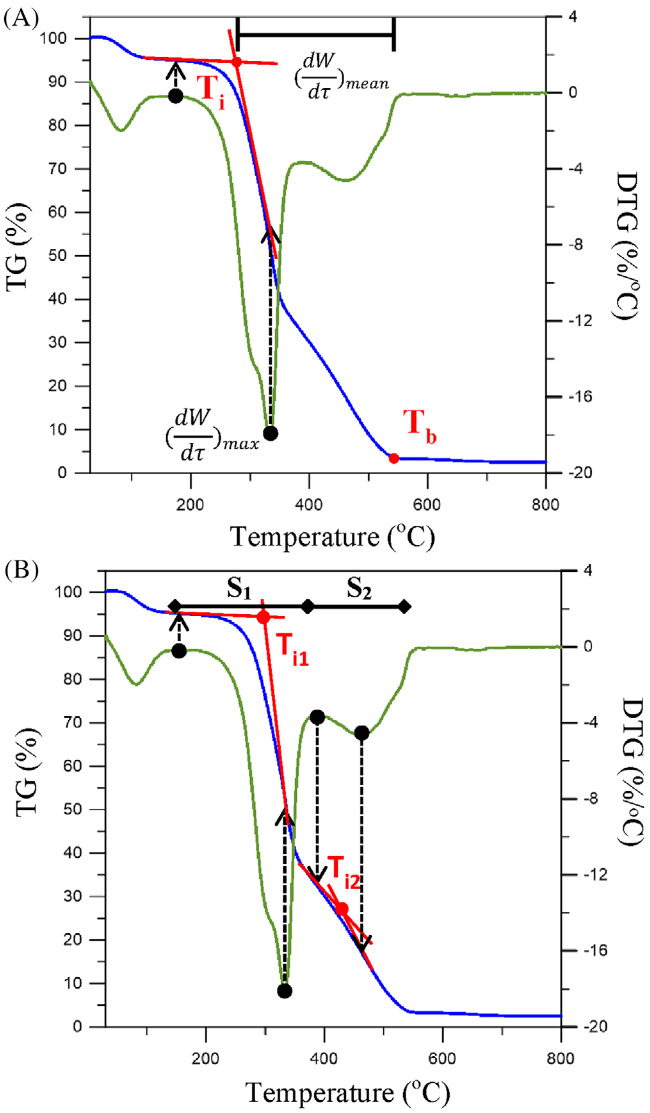

FIGURE 5 (A) Method for defining ignition temperature, and (B) determination of volatile matter reaction stage and fixed carbon reaction stage. *Note*: Blue line denotes the curve of thermogravimetry and green line denotes the curve of DTG [Colour figure can be viewed at wileyonlinelibrary.com]

$$\alpha = \frac{W_i - W}{W_i - W_f} \times 100\%, \tag{5}$$

where $\boldsymbol{W_i}$ and $\boldsymbol{W_f}$ are the initial and final weights of the biomass, respectively.

However, the maximum weight loss of biomass usually occurs at the stage of VM combustion, and the VM is ignited at the ignition temperature. It seems, therefore, that the performance of VM combustion is dominant. In other words, the effect of FC combustion on the overall combustion feature is negligible. However, the results of the weight loss curve exhibit two stages of decline with increasing environmental temperature. The two segments of the decline in the weight loss curve are shown in Figure 5B. The comprehensive combustion characteristic index was divided into two portions, namely the VM reaction stage (S_1) and the FC reaction stage (S_2). However, the T_i value obtained with the cross method cannot represent the ignition temperature of biochar because the slopes of the two segments (denoted S_1 and S_2 in Figure 5B) would introduce measurement bias and uncertainty in the determination of the ignition temperature with the cross method. T_{i1} and T_{i2} shown in Figure 5B refer to the ignition temperature of biochar during S_1 and S_2 periods. For accurate determination with the cross method, the two segment slots on the weight loss plot must be considered individually. Consequently, a modified method for calculation of the S index was proposed.

Notably, the ignition temperature and the maximum and average DTG values correspond to the respective stages. The value of burnout temperature, however, is independent to the variation of TG signal. The burnout temperature was determined while it comes to 99% fuel conversion rate. Then, based on the weight loss percentage in each stage, an effective comprehensive combustion characteristic index can be obtained as follows,

$$S_{\text{mix}} = S_1 \times \frac{W_1}{W_1 + W_2} + S_2 \times \frac{W_2}{W_1 + W_2} \tag{6}$$

where W_1 and W_2 denote weight loss percentages during S_1 and S_2 periods, respectively.

3.1.3 | Proximate analysis-based index

Proximate analysis is one of the major methods for analyzing the chemical properties of substances. Through proximate analysis, M, ASH, VM, FC can be determined. For proximate analysis, in this study, the sample was undertaken for 1 hour of heating with 105°C inert atmosphere. This heating stage facilitated the removal of the M content in the fuel. The weight loss of the sample is equivalent to the M percentage in the fuel. Sequentially, the sample was conducted for 7 minutes of heating with 950°C inert atmosphere, leading to the release of VM due to the pyrolysis reaction. The VM percentage of the fuel can be examined on the basis of the change in the weight of the fuel. Once the diluent gas was changed from nitrogen to air, a combustion reaction commenced. Ultimately, ASH remained in the residue. The total program is drawn in Figure 6. The ASH content of a fuel sample is the retained weight percentage of the sample after it is placed in a furnace and heated to 750°C at a heating rate of 20°C/min. The FC content can be determined by subtracting the sum of M, VM, and ASH from 100%:

$$\text{FC}(\%) = 100 - (M + \text{VM} + \text{ASH}). \tag{7}$$

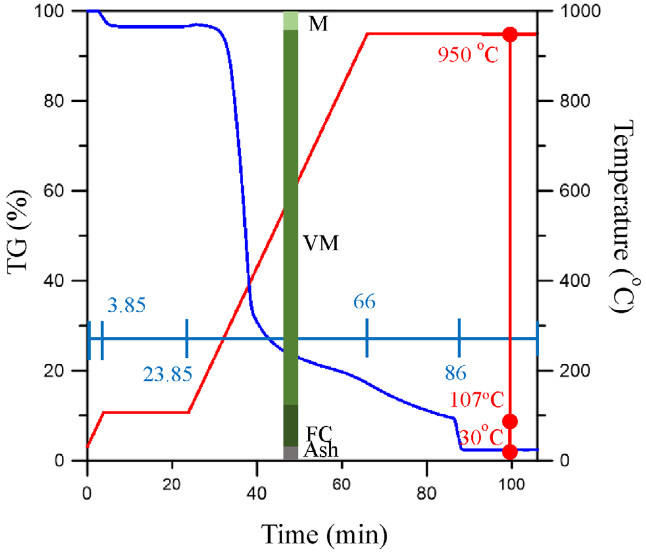

FIGURE 6 Determination of temperature program and percentage of proximate analysis [Colour figure can be viewed at wileyonlinelibrary.com]

In this study, the proximate analysis was conducted with TGA. The temperature graph is denoted by the red line in Figure 6. The initial conditions of the experiment were ambient temperature of 30°C and nitrogen atmosphere. The heating program was as follows: heat from 30°C to 107°C, hold at 107°C for 20 minutes, heat again from 107°C to 950°C, and hold at 950°C for 20 minutes. After fulfillment of the above procedure, the inert gas was replaced with air. Heating for 20 minutes in air would burn out all combustible gases in the product, but ASH would remain.

Different contents of proximate analysis differently influence combustion characteristics. Biomass with a high VM content has a significantly low ignition temperature. The HHV of a biofuel is contingent on its FC content. Contrariwise, M content absorbs exothermic heat, and ASH affects radiative heat transfer and may cause corrosion.[35] Moisture content and ASH content are unfavorable for combustion, but VM and FC contents are favorable. The proximate-analysis-based index was developed in an attempt to anticipate the combustion behavior of a fuel on the basis of the observations made in the proximate analysis. Therefore, the proposed index for the Taguchi method is the fraction of the product of VM and FC to the product of M and ASH.[14]

$$\text{PA} = \frac{\text{VM} \times \text{FC}}{M \times \text{Ash}}. \tag{8}$$

3.2 | Taguchi method optimization

To scrutinize the optimum condition for torrefaction, we used the Taguchi method.[14,36] This method employs S/N ratio as the quality characteristic of selection. The S/N ratio is applied as a measurable value instead of a SD[37] and expressed as follows, where n is the number of total experiments, and y_i is the value to be analyzed, for example, the values of EY, PA, and S_{mix}:

$$\mathrm{S/N} = -10\log\left[\frac{1}{n}\sum_{i=1}^{n}\frac{1}{{y_i}^2}\right]. \tag{9}$$

In selecting the parameters to create the orthogonal array, we focused on the influence of temperature. According to Reference 38, temperature is the most dominant parameter influencing torrefaction, followed by residence time and carrier gas flow rate. The torrefaction temperature ranges from 200 to 300°C, and six temperature values from this range were used in the optimization herein: 200, 220, 240, 260, 280, and 300°C. The general residence time for torrefaction was set to 10 to 60 minutes,[38] and the residence times of 20, 40, and 60 minutes were selected for optimization. The flow rate of nitrogen gas was calculated as the rate of passage of N_2 through the biomass.

The total length of the tubular high-temperature furnace was 30 cm, and its cross-sectional area was 10.75 cm^2. The heating rate of the tubular furnace was 20°C/min. The particle weight of biomass was 15 ± 1 g with particle size ranging from 425 to 880 μm. Thus, three flow rates were selected for the optimization, 30, 50, and 70 mL/min, respectively. Each of the three parameters, incorporating temperature, residence time, and nitrogen gas flow rate, had three levels, resulting in the following orthogonal array: $L_{18}(6^1 \times 3^6)$. The 18-experiment matrix is shown in Table 2.

Once all experiments were completed, the S/N ratios of the results were determined. Then, we obtained the average effects of the parameters at different levels, that is, averaging the S/N ratio of each parameter at each level. The maximum value represented the best level for the corresponding parameter. The rank represents the effect of different parameters on the indexes, which was calculated as the maximum value minus the minimum value. The greater the difference was, the stronger the influence was.

TABLE 2 Experimental layout using L_{18} orthogonal array

No.	Temperature (°C)	Residence time (minutes)	N_2 flow rate (mL/min)
1	200	20	30
2	200	40	50
3	200	60	70
4	220	20	30
5	220	40	50
6	220	60	70
7	240	20	50
8	240	40	70
9	240	60	30
10	260	20	70
11	260	40	30
12	260	60	50
13	280	20	50
14	280	40	70
15	280	60	30
16	300	20	70
17	300	40	30
18	300	60	50

3.3 | Optimization results

3.3.1 | Energy yield

The analysis results for EY are shown in Table 3. Torrefaction reduces product weight but increases the HV. The product of the ratio of weight change and the change in HV before and after torrefaction is smaller than 1. This means the total inherent energy of the biomass decreased after thermal degradation. However, there are two kinds of densities, that is, apparent density and bulk density. The apparent density was determined as the ratio of the pellet mass to its volume; whereas the bulk density was determined as the ratio of the mass to the volume. It is worth noting that the apparent energy density and bulk energy density of torrified feedstocks can be either higher or lower than that of untreated ones, depending on the nature of the properties of the parent feedstock, as experimentally demonstrated by Brachi et al.[39] Furthermore, its energy density increased, meaning that the energy per unit weight of biochar increased. The reduced weight of the biochar makes it easy to transport and store. From the results, EY decreased as the torrefaction temperature increased. The optimal temperature for maximizing EY was 200°C, as indicated by item number 3 in Table 3. This set of experiments yielded the largest value of the EY index, which corresponds to the lowest operating temperature. Residence time and carrier gas flow rate did not exhibit noteworthy trends.

The S/N ratio of each parameter at each level was determined by averaging the S/N ratios obtained for that parameter. For example, the S/N ratio at 200°C was computed by averaging the S/N ratios obtained in the

TABLE 3 Experimental results and signal-to-noise (S/N) ratio based on EY index

NO.	Initial weight (g)	Final weight (g)	Heating value (kM/kg)	EY × 100 (%)	$(S/N)_{EY}$ (−)
1	16.12	14.84	18 188.56	93.32	−0.83
2	15.77	14.52	18 569.22	94.68	−0.65
3	13.63	12.62	18 441.06	95.70	−0.66
4	15.04	13.69	18 793.90	95.07	−0.65
5	13.97	12.48	19 067.99	94.21	−0.68
6	14.49	13.24	18 773.23	94.95	−0.62
7	15.36	13.35	19 163.72	92.83	−0.88
8	15.55	13.30	19 483.21	92.25	−0.87
9	14.65	12.57	19 770.61	93.99	−0.72
10	15.55	12.66	19 837.18	87.66	−1.14
11	13.11	9.96	20 245.2	83.43	−1.57
12	14.32	10.77	21 487.48	87.67	−1.14
13	14.11	9.86	21 467.60	81.38	−1.79
14	15.03	10.20	21 447.14	78.98	−2.05
15	13.20	9.24	21 665.55	82.30	−1.69
16	15.36	9.02	23 872.27	76.11	−2.37
17	15.51	8.77	24 297.79	74.56	−2.55
18	15.22	8.56	25 296.21	77.21	−2.25

experiments conducted at 200°C, namely numbers 1, 2, and 3 in Table 3. By averaging −0.83, −0.65, and −0.66, we obtained the value of −0.713, which is the S/N value of the level 1 torrefaction temperature, as given in Table 4. As for the S/N ratio of the residence time of 20 minutes, the S/N ratio values corresponding to numbers 1, 4, 7, 10, 13, and 16 were averaged. In Table 4, the maximum S/N of temperature is −0.65 at 220°C, which is different from the experimental results obtained herein. This discrepancy was ascribed to the fact that none of the above experimental results are identical to the theoretically optimal results. The maximum value of torrefaction residence time was located at L3, as indicated in Table 4, and the value was 60 minutes. In terms of the nitrogen carrier gas flow rate, level 2 yielded the best result of 50 mL/min. The difference in S/N was determined by

TABLE 4 Signal-to-noise (S/N) ratio for each level based on EY index

	$(S/N)_{EY}$		
	Temperature	Res. time	N_2 flow rate
*L*1	−0.71	−2.55	−2.67
*L*2	−0.65	−2.79	−2.46
*L*3	−0.82	−2.36	−2.57
*L*4	−1.29	—	—
*L*5	−1.84	—	—
*L*6	−2.39	—	—
Max value	−0.65	−2.36	−2.46
Min value	−2.39	−2.79	−2.67
S/N difference	1.74	0.43	0.21
Ideal condition	220 (°C)	60 (minutes)	50 (mL/min)

subtracting the maximum S/N from the minimum S/N. Taking temperature as an example, the S/N difference is the maximum value −0.65 minus the minimum value −2.39, and it is equal to 1.74. Because torrefaction temperature has the largest S/N difference, it is the dominant factor among the factors considered in the analysis. Residence time is the second most important factor, and N_2 flow rate is the least important factor. The ideal torrefaction parameters are torrefaction temperature of 220°C, the residence time of 60 minutes, and N_2 flow rate of 50 mL/min. Because the ideal torrefaction conditions (torrefaction temperature of 200°C, the residence time of 60 minutes, and N_2 flow rate of 50 mL/min) do not match any set of experimental parameters, a confirmation experiment should be conducted to validate the theoretical and experimental outcomes.

To confirm the accuracy of the optimal parameters, a confirmation experiment was conducted according to the parameters to compare the results. The theoretical S/N value was −0.313, which means that the EY was 96.46. In the confirmation experiment, the EY was 99.09, which was higher than the values obtained in all experiments. The theoretical and experimental outcomes of EY differed by 2.64%, but the difference was suitably small for assuming that the optimal result was correct.

3.3.2 | Effective comprehensive combustion index

The weight percentages in stages 1 and 2 are complementary, accounting for approximately 92% of the entire amount of material. The decrease in VM was not evident at low torrefaction temperatures, but as the temperature increased to 260°C and higher, VM decreased exponentially. The decrease of VM resulted in the increase of the FC content, which is the main component governing heat generation. Even though the VM content of the biochar torrefied at 300°C was considerably lower than that of raw biomass, the VM percentage was similar or even marginally higher than that of coal. The ASH content was considerably lower than that of coal, which means fewer cleaning processes would be required after combustion. The maximum weight loss and average weight loss in both stages exhibited no obvious trends. The ignition temperature in stage 1 increased as the torrefaction temperature increased because the VM content decreased after thermal treatment. However, the ignition temperature of the FC varied from 353 to 486°C. In addition, the burnout temperature was affected by the torrefaction temperature, and it exhibited a gradual rising trend in Table 5. Overall, the S_{mix} index showed better results when the torrefaction temperature was moderate because the ignition temperature accounts for a square in the index, as shown in Table 5. At very high torrefaction temperatures, the ignition temperature would increase, which is unfavorable for ignition of biomass during combustion. The trend of burnout temperature increased as well, accounting for a cause S_{mix} index decrease.

The S/N ratios corresponding to each level are shown in Table 6. According to these values, temperature had the strongest influence. The differences among the low torrefaction temperatures were not significant, and the maximum value corresponding to level three was 240°C. However, as the torrefaction temperature increased to 260°C and beyond, this index worsened. Residence time had the weakest effect on the S index, meaning that the S/N ratios corresponding to the various levels were very similar. The optimal temperature, residence time, and N_2 flow rate were 240°C, 60 minutes, and 70 mL/min, respectively, as shown in Table 6. Confirmation experiments were conducted to examine the accuracy of the optimal condition. The theoretically optimal S/N ratio was 30.46, and the corresponding S index was 33.33. The experimental S/N value of the parameters was 28.17, which is marginally lower than the theoretical value but higher than all orthogonal array results.

3.3.3 | Proximate analysis-based index

The proximate analysis-based index (PA) depends on the ratio of the product of VM and FC to the product of M and ASH. The experimental results are shown in Table 7. The index is larger when the product of VM and FC is larger and the product of M and ASH is smaller. As a result, M varied from 1% to 3%, and ASH varied from 1% to 3%. These two proportions did not change considerably, thus implying that the index was mostly contingent on the product of VM and FC. Mathematically, under the circumstances of the same sum, if maximizing the multiplication of two numbers, those numbers should be quite equal. For raw alee trees, VM accounted for almost 95% of the raw biomass by weight, which left an FC of only 2%. The gap between VM and FC was certainly large, resulting in a small product. As the degree of torrefaction increased, the proportion of VM decreased gradually. However, even at the torrefaction temperature of 300°C, VM accounted for approximately 60% of the raw biomass by weight. However, the difference between VM and FC decreased. As a result, the PA index yielded a higher degree of torrefaction.

According to the calculated S/N ratios at each level, as shown in Table 8, temperature has a stronger

TABLE 5 Experimental results and signal-to-noise (S/N) ratio-based S_{mix} index

Number	Ignition 1 (°C)	Ignition 2 (°C)	Burnout (°C)	Weight W_1 (%)	Weight W_2 (%)	Max S_1 (−)	Max S_2 (−)	Mean S_1 (−)	Mean S_2 (−)	S_{mix} (−)	$(S/N)_{S\,\mathrm{mix}}$ (−)
1	288.16	443.29	563.03	64.93	28.63	20.08	4.88	4.73	288.16	14.53	23.24
2	285.61	369.29	533.43	66.19	28.30	20.30	5.05	5.82	285.61	19.86	25.96
3	281.50	437.16	534.09	64.91	28.01	19.28	4.89	5.99	281.50	19.62	25.85
4	293.91	353.81	539.29	63.97	29.76	19.37	4.96	5.93	293.91	17.78	25.00
5	283.61	448.81	547.48	63.92	29.83	19.56	4.76	5.38	283.61	16.82	24.52
6	294.12	436.16	535.55	62.13	31.52	20.49	5.12	6.15	294.12	18.72	25.44
7	303.31	448.90	563.42	64.42	29.75	22.92	4.56	5.67	303.31	17.62	24.92
8	300.84	438.36	543.73	64.65	30.63	24.35	5.07	5.66	300.84	19.68	25.88
9	302.20	458.72	567.07	61.87	32.80	23.75	4.83	8.85	302.20	27.07	28.65
10	310.66	476.46	581.66	62.51	33.37	24.07	4.81	5.17	310.66	14.94	23.49
11	315.54	466.50	604.31	57.74	37.62	23.73	4.96	4.83	315.54	12.12	21.67
12	315.90	467.51	603.53	57.45	38.25	23.86	5.07	4.87	315.90	12.18	21.71
13	315.64	472.48	615.29	52.68	43.56	21.86	5.47	5.38	315.64	11.25	21.02
14	312.11	468.42	627.42	47.64	47.38	20.19	5.31	4.91	312.11	8.91	19.00
15	315.23	477.37	634.00	49.43	45.53	20.32	5.22	4.99	315.23	9.07	19.16
16	309.10	463.16	677.55	30.99	64.28	12.25	5.58	3.59	309.10	2.91	9.27
17	305.97	486.25	694.25	28.02	67.17	10.35	5.84	3.51	305.97	2.70	8.63
18	307.44	457.45	690.85	26.95	67.49	9.62	5.76	2.08	307.44	2.07	6.33

TABLE 6 Signal-to-noise (S/N) ratio for each level based on S_{mix} index

	$(S/N)_{S\mathrm{mix}}$		
	Temperature	**Res. Time**	**N_2 flow rate**
*L*1	25.02	42.31	42.12
*L*2	24.99	41.89	41.49
*L*3	26.48	42.38	42.98
*L*4	22.29	—	—
*L*5	19.73	—	—
*L*6	8.08	—	—
Max value	26.48	42.38	42.98
Min value	8.08	41.89	41.49
S/N difference	18.40	0.49	1.49
Ideal condition	240 (°C)	60 (minutes)	70 (mL/min)

influence than residence time and carrier gas flow rate. However, in this case, the impact of residence time was more important than that of N_2 flow rate. The optimized outcome was torrefaction temperature of 300°C, residence time of 60 minutes, and carrier gas flow rate of 70 mL/min. The results of the confirmation experiments were only 2% superior to the results of the 17th experiment. Even so, the theoretically calculated results represent the optimal operating parameters.

4 | OPTIMIZATION OF COMBUSTION BEHAVIOR

4.1 | Taguchi method optimization

4.1.1 | Parameter selection and setting

All parameters pertaining to the optimization of fluidized-bed combustion were selected from the

TABLE 7 Experimental results and signal-to-noise (S/N ratio) based on proximate analysis-based index (PA)

Number	*M* (%)	Ash (%)	VM (%)	FC (%)	PA (%)	$(S/N)_{PA}$ (−)
1	2.54	1.43	94.15	1.88	48.81	33.77
2	1.87	2.44	91.61	4.08	80.62	38.13
3	2.92	1.74	90.73	4.61	82.62	38.34
4	1.49	1.56	92.47	4.48	179.10	45.06
5	2.44	2.29	88.47	6.80	107.24	40.61
6	1.66	1.53	91.64	5.17	187.55	45.46
7	1.85	2.68	81.97	13.50	222.69	46.95
8	1.83	2.20	82.81	13.16	269.90	48.62
9	1.84	2.25	81.01	14.90	291.61	49.30
10	1.02	1.73	87.02	10.23	503.57	54.04
11	1.27	2.89	76.08	19.76	409.08	52.24
12	1.00	2.02	75.77	21.21	792.26	57.98
13	1.30	3.21	74.54	20.95	374.46	51.47
14	0.76	2.15	69.13	27.96	1186.79	61.49
15	1.09	2.15	70.87	25.89	785.87	57.91
16	1.01	2.59	63.95	32.45	793.16	57.99
17	0.74	2.55	60.22	36.49	1172.00	61.38
18	0.93	1.67	73.11	24.	1143.73	61.17

TABLE 8 Signal-to-noise (S/N) ratio for each level based on proximate analysis-based index (PA)

	$(S/N)_{PA}$		
	Temperature	**Res. time**	**N_2 flow rate**
*L*1	36.75	96.43	99.89
*L*2	43.71	100.82	98.77
*L*3	48.29	103.39	101.98
*L*4	54.75	—	—
*L*5	56.96	—	—
*L*6	60.18	—	—
Max value	60.18	103.39	101.98
Min value	36.75	96.43	98.77
S/N difference	23.43	6.96	3.21
Ideal condition	300 (°C)	60 (minutes)	70 (mL/min)

experimental testing results. The first parameter was the height of the bed zone. There is a certain range of ideal bed height; if the bed is too deep, the slugging phenomenon will occur, which is undesirable with respect to uniform mixing. The occurrence of slugging depends on the ratio of bed height to bed diameter. Usually, when this ratio is large, slugging can be observed. Because the diameter of the fluidized bed was 55 mm, silica sand, the volume and weight of which were 190 mL and 180 g, respectively, was filled into the fluidized bed up to 50 mm as the bed material. The second parameter was the fluidization velocity. Fluidization velocity is usually several times the minimum fluidization speed. The ideal fluidization velocity should be 1.5 times higher than the minimum fluidization speed.[40] In the visualization experiments, when air was introduced at a superficial gas velocity of approximately 0.018 m/s, air bubbles began to be generated in the sand bed, which can be defined as the minimum fluidization. Because the minimum gas velocity of fluidization was 0.018 m/s, the best fluidization velocity was approximately 0.028 m/s (0.018 × 1.5). The third parameter was the thermocouple position.

4.1.2 | Orthogonal array construction

The parameters used to construct the orthogonal array used in Taguchi method optimization were selected. In this optimization experiment, four parameters were considered, namely operating bed temperature, torrefied materials, oxygen concentration, and second oxygen inlet position. In most industrial applications, the temperature of the fluidized bed is maintained in the range of 750 to 1000°C, but the biomass briquettes yield volatile gas while the bed temperature of fluidized-bed reactor ranges from 200 to 700°C. For combusting biomass, we set a lower temperature to avoid bed agglomeration. According to the visualization experiments, the waste wood pellets ignited at the bed temperature of 535°C. Because biomass can be ignited at a lower temperature, 550 and 650°C were selected to investigate whether lower temperatures are feasible for combusting biomass in a fluidized bed. The typical fluidized bed operating temperature was set to 750°C. For oxygen-enriched combustion, Wu et al found that as the oxygen concentration was raised from 21% to 30%, the fuel consumption reduced by 26%,[41] and Huynh and Kong discussed the combustion and NO_x emission of biomass-derived syngas with 21%, 30%, and 40% oxygen-enrichment levels.[42] It implies that the presence of oxygen-enrichment can facilitate the combustion of biomass-derived syngas and hydrocarbon fuels. In the present study, we investigated three points in this range of oxygen concentrations, which were 23%, 27%, and 30%. As for the different degrees of torrefaction of the biomaterial, EY optimization, S_{mix} index optimization (SI), and PA optimization were selected. The parameter of oxygen inlet position was selected on the basis of the reasons mentioned in the previous paragraph. Each parameter had three levels, so an L_9 (3^4) orthogonal array was constructed, as shown in Table 9.

4.1.3 | Optimization parameters

Combustion consists of four stages: water evaporation, pyrolysis (devolatilization), volatile burning, and char combustion. When fuel is fed into a combustion chamber, its moisture content is first evaporated. Then, large complex hydrocarbon molecules are broken down into smaller molecules such as CO, H_2, and CH_4 due to the high temperature in the bed zone, which is the process of pyrolysis. As the temperature reaches the ignition temperature, flames appear, and volatile combustion commences. The combustion of volatile gases provides adequate heat to trigger char combustion. The char combustion stage accounts for most of the combustion time.

4.1.4 | Total fluidized bed efficiency

In terms of combustion efficiency, many aspects can be defined and explored. In this research, the total efficiency of the fluidized bed was investigated. The Poisson index is designed to represent the condition of the boiler. The ratio has been proved to be a reliable indicator of burner health. It uses the composition of the flue gas to determine whether a burner is in good condition or needs to be repaired or overhauled. The index is expressed mathematically in Equation (11) as the ratio $CO:CO_2$. The values of this index for a clean boiler, a boiler that needs cleaning, and a boiler that needs an overhaul will be less than 0.4%, between 0.4% and 0.8%, and greater than 0.8%, respectively.

$$PI\% = 100 \times \left({}^{CO}\!/_{CO_2} \right). \tag{11}$$

TABLE 9 Orthogonal array for optimizing combustion

	Bed temperature (°C)	Materials (–)	Oxygen position (cm)	Oxygen concentration (v%)
1	550	EY	0	23
2	550	SI	45	27
3	550	PA	55	30
4	650	EY	45	30
5	650	SI	55	23
6	650	PA	0	27
7	750	EY	55	27
8	750	SI	0	30
9	750	PA	45	23

4.1.5 | Volatile combustion ratio

However, the combustion process of biomass fuels can be classified into two phases: the volatile combustion phase (phase 1) and char combustion phase (phase 2). The water evaporation stage and pyrolysis stage are included in the volatile phase because the time required for each of these stages is short and the two stages overlap each other. The demarcation point between phases 1 and 2 is the point at which the flame goes out. The volatile combustion ratio (V-CR) equation is expressed as follows.

$$\mathrm{V-CR\%} = 100 \times (\mathrm{CO} + \mathrm{CH_4})/(\mathrm{CO} + \mathrm{CO_2} + \mathrm{CH_4}). \quad (12)$$

4.2 | Optimization results

4.2.1 | Total fluidized bed efficiency

To determine the total combustion efficiency of the fluidized bed, the overall emissions of CO and CO_2 were calculated by integrating the corresponding data curves. The calculated total values of CO and CO_2 in each experiment are shown in columns 1 and 2 of Table 10. The value of CO indicates that the oxygen inlet position significantly influenced the generation of CO. CO concentration decreased when oxygen was injected with the carrier gas from the bottom of the fluidized bed. This is because the oxygen passed through the bed zone, where most of it was consumed. Placement of the oxygen inlet after the bed zone was less effective in combusting the generated CO, resulting in a higher concentration of CO in the exhaust gas. Bed temperature and the difference in torrefied materials had rather weak effects on total combustion efficiency of the fluidized bed. By examining the CO_2 values, it is evident that the trend of change in CO_2 was similar to that of CO. As the amount of CO increased, so did the amount of CO_2. This is because when a greater amount of CO was generated, it was burned downstream to form CO_2. However, under certain conditions, the concentration of CO_2 was high but that of CO was low. This phenomenon was observed in experiment number 3 and may be ascribed to the fact that the oxygen inlet was in the flame zone and the O_2 concentration was higher, which enhanced the volatile combustion.

The high amount of CO may be ascribed to a more severe pyrolysis reaction or to weak combustion in the freeboard zone. Thus, observing only the change in either CO concentration or CO_2 concentration is inadequate, and the result may be misleading. By dividing CO with CO_2 to obtain the Poisson index, the trend can be

TABLE 10 Experimental results and signal-to-noise (S/N) ratio based on PI index

NO.	CO (ppm-min)	CO_2 (ppm-min)	PI (%-min)	$(S/N)_{PI}$ (−)
1	1 288 021	645	0.199693	−13.99274
2	1 494 872	945.8	0.158054	−16.02391
3	1 176 454	1216.4	0.096716	−20.29003
4	1 862 043	815.1	0.228444	−12.82442
5	2 202 569	942.7	0.233645	−12.62888
6	1 012 813	679.4	0.149075	−16.53193
7	1 010 427	652.8	0.154784	−16.20550
8	692 784	321.3	0.215619	−13.32626
9	1 951 594	1078.9	0.180887	−14.85183

TABLE 11 Signal-to-noise (S/N) ratio for each level based on PI index

	$(S/N)_{PI}$			
	Bed temperature	**Materials**	**Oxygen position**	**Oxygen concentration**
*L*1	−16.77	−14.34	−14.62	−13.82
*L*2	−13.99	−13.99	−14.57	−16.25
*L*3	−14.79	−17.23	−16.38	−15.48
Max value	−13.99	−13.99	−14.57	−13.82
Min value	−16.77	−17.23	−16.38	−16.25
S/N difference	2.78	3.24	1.81	2.43

visualized more clearly. The results of the Poisson index and the S/N ratios are shown in Table 10. In the analysis of this set with the Taguchi method, the smaller-the-better characteristic was adopted because the generation of a smaller amount of CO and a larger amount of CO_2 indicates cleaner combustion. Based on the experimental results, the conditions associated with experiment number 3, which had the lowest Poisson index and the smallest S/N ratio (= −20.29), appear to be the best conditions. The optimal experimental conditions were a bed temperature of 550°C, torrefied materials according to the PA, an oxygen inlet position at freeboard area, and an oxygen concentration of 30%.

Table 11 shows the calculated S/N ratios of each factor at each level. The minimum value of each factor represents the theoretically optimal operating conditions. In terms of bed temperature, lower temperatures seem to result in performance superior to higher temperatures, so the optimal result is 550°C. In terms of the fed materials, a higher degree of torrefaction, namely the PA, yields the best results. Superior results were achieved when oxygen was injected into the freeboard downstream of the fluidized bed at a concentration of 27%. Because the optimal results differ from the results of the nine sets of experiments listed in the orthogonal array, confirmation experiments should be conducted to verify the authenticity of the optimization procedure. We operated the experiment with theoretically optimal parameters and obtained a Poisson index of 0.095%, which is smaller than that obtained in experiment number 3. The S/N ratio was −20.43, meaning that the optimal results were correct and this set of Taguchi method optimization could be implemented.

4.2.2 | Volatile combustion ratio

The volatile combustion and char combustion stages were demarcated on the basis of the existence of a flame in the combustion zone. Although the fluidized bed was made of stainless steel and it was not possible to see the flame directly, the existence of the flame was detected with T3, which was located at the center of the freeboard zone. When the flame appeared, the thermocouple reading increased instantly, and when the flame disappeared, the thermocouple reading decreased instantly. When compared with the timeline of flue gas, take experiment number 1, which is shown in Table 8, as an example: the curve matches the CO_2 trend, which is reasonable because carbon dioxide was generated mostly because of

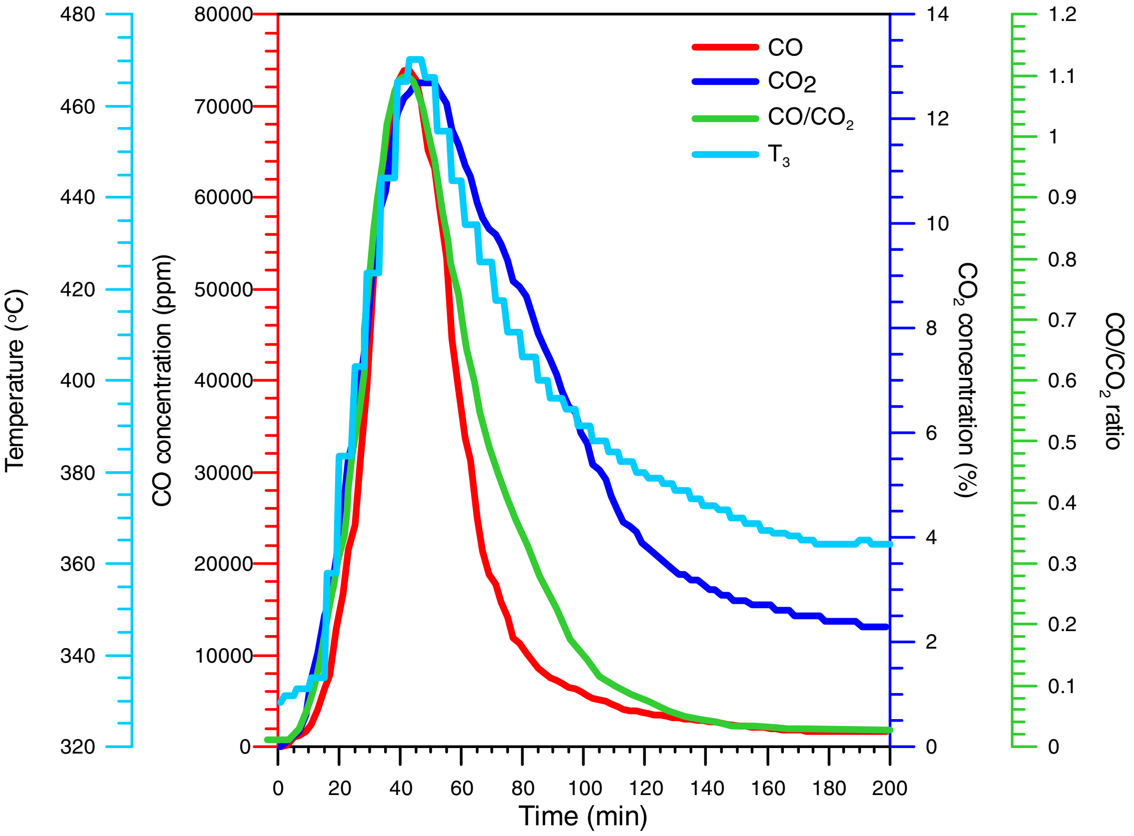

FIGURE 7 Comparison of CO, CO_2, CH_4, and T3 temperature [Colour figure can be viewed at wileyonlinelibrary.com]

TABLE 12 Experimental results and signal-to-noise (S/N) ratio based on V-CR index

NO.	CO (ppm-min)	CO_2 (%-min)	CH_4 (%-min)	$CO + CH_4/CO + CH_4 + CO_2$ (−)	$(S/N)_{V\text{-}CR}$ (−)
1	675 605	121.7	15.231	0.115594778	−18.74124
2	580 849	147.6	11.868	0.077781559	−22.18247
3	232 708	213.5	7.521	0.035044421	−29.10762
4	823 620	163.9	25.246	0.137230469	−17.25099
5	1 016 494	209.4	53.335	0.206070848	−13.71967
6	255 522	77.9	5.739	0.07145308	−22.91958
7	416 718	149	17.672	0.108258165	−19.31079
8	327 723	63	7.271	0.107632584	−19.36112
9	698 365	112.1	30.009	0.21502648	−13.35016

TABLE 13 Signal-to-noise (S/N) ratio for each level based on Volatile combustion ratio (V-CR) index

	$(S/N)_{V\text{-}CR}$			
	Bed temperature	**Materials**	**Oxygen position**	**Oxygen concentration**
*L*1	−23.34	−18.43	−20.34	−15.27
*L*2	−17.96	−18.42	−17.60	−21.47
*L*3	−17.34	−21.79	−20.71	−21.91
Max value	−17.34	−18.42	−17.60	−15.27
Min value	−23.34	−21.79	−20.71	−21.91
S/N difference	6.00	3.37	3.11	6.64

volatile combustion. Therefore, the point distinguishing the two stages was the maximum temperature reading of T3, which represented the maximum CO_2 concentration as well.

The generation of CO and CH_4 exhibited the same trends and peaks along the timeline, as shown in Figure 7. Based on this result, it can be speculated that both CO and CH_4 were generated by the pyrolysis reaction. The experimental results are shown in Table 12. Different degrees of torrefied materials had a major influence in this experiment. Materials with a lower degree of torrefaction contained more volatile matter and were easier to devolatilize. Oxygen concentration was important as well because pyrolysis often occurs under low oxygen concentrations in the carrier gas. The CO_2 curve was marginally delayed compared to the CO and CH_4 curves, but its peak corresponded to the temperature reading of T3. Oxygen inlet position had the strongest influence on CO_2 generation. The CO_2 concentration increased when oxygen was injected downstream of the combustion chamber. One can surmise that the extra oxygen in the freeboard zone enhances the burning process.

In terms of the optimization of the results of each factor, Table 13 shows that at lower bed temperatures, the volatile combustion ratio is smaller; it is superior according to our definition because less unburnt carbons were in the flue gas. For the biomaterials considered herein, the PA degree of torrefaction was the best. The ratio of oxygen concentration was higher at the oxygen concentration of 23%, but it was lower at the oxygen concentrations of 27% and 30%. There was no obvious difference between 27% and 30%, which means that an oxygen concentration above 27% was enough.

The optimal experimental and theoretical results were identical. For bed temperature, 550°C was the most effective. The PA was superior in terms of the volatile combustion ratio. The optimal oxygen inlet position was in the freeboard zone, which was at a height of 55 cm. A higher oxygen concentration, 30% in this study, yielded the best results.

5 | CONCLUSION

The primary purpose of this study was to optimize the combustion efficiency of a fluidized bed fed with torrefied biomass. The Taguchi method was adopted as the optimization approach because of its high accuracy and efficiency. Torrefied biochar was used as the biomass material to explore the effect of thermal pretreatment on combustion characteristics in a fluidized-bed reactor. Different percentages of oxygen were injected into the combustion chamber at different positions to investigate oxygen-enriched lancing.

The first half of this research focused on optimization of the biomass in terms of the energy stored in biochar (EY), material analysis of biochar (PA), and combustion behavior of biochar (S_{mix}). Three parameters were controlled, namely torrefaction temperature, torrefaction residence time, and N_2 carrier gas flow rate. Overall, torrefaction temperature was dominant in this set of Taguchi method optimization experiments. The residence time exhibited the same trend whereby a longer torrefaction time, 60 minutes in this study, was more effective for converting raw biomass into biochar. The N_2 flow rate had no significant impact on the conversion of biochar. The optimal results of each index were carried forward into the second part of this research.

The second part of this study involved the optimization of the combustion efficiency of the fluidized bed. Four parameters, namely the temperature of the fluidized bed, different degrees of biochar torrefaction, different oxygen concentrations, and different positions of the second oxygen injection, were incorporated into the constructed Taguchi orthogonal array to obtain the optimal results from aspects of two ratios, the ratio of CO to CO_2 (Poisson index) and the ratio of unburnt carbon (CO and CH_4) to total flue gas (CO, CH_4, and CO_2), respectively. In terms of the total combustion efficiency of the fluidized bed, the degree of torrefaction of the biomaterials had the strongest influence, and bed temperature and oxygen concentration were equally important. Oxygen inlet position had the weakest influence on combustion efficiency. In terms of the volatile combustion ratio, bed temperature and oxygen concentration were important, and degree of torrefaction of the biomaterials and oxygen inlet position were less important. The optimal results for both total fluidized-bed combustion efficiency and volatile combustion ratio were mostly the same, differing marginally in terms of the oxygen concentration. From an analysis of the S/N values, 27% is the most effective concentration for boiler efficiency, and 30% is the most effective for volatile combustion. In sum, compared with the experiments without oxygen enrichment, superior results were achieved with oxygen enrichment.

ACKNOWLEDGEMENTS

This work was financially supported by the Ministry of Science and Technology (Republic of China, Taiwan) under grant numbers MOST 106-2923-E-006-003-MY3, MOST 106-3113-E-006-002-CC2, and MOST 108-2628-E-006-008-MY3. The authors wish to thank Dr. Yei-Chin Chao and Dr. Guan-Bang Chen for their technical advice.

NOMENCLATURE

ASH	Ash
$\left(\frac{dW}{d\tau}\right)_{max}$	Maximum weight loss rate
$\left(\frac{dW}{d\tau}\right)_{mean}$	Average weight loss rate
EY	Energy yield index
FC	Fixed carbon
HV	Heating value
k	Quality loss constant
M	Moisture
m	Target value
PA	Proximate analysis-based index
PI	Poison index
Q	Average quality loss
S	Combustion comprehensive index
S_1	Stage one of S_{mix}
S_2	Stage two of S_{mix}
S_{mix}	Effective combustion comprehensive index
T_b	Burnout temperature
T_i	Ignition temperature
V-CR	Volatile combustion ratio
VM	Volatile matter
W_i	Initial weight
W_f	Final weight
$y_i;\bar{y}$	Actual value; average actual value
α	Fuel conversion rate
σ^2	Variance of the actual value

ORCID

Yueh-Heng Li https://orcid.org/0000-0003-0458-1300

REFERENCES

1. Malinauskaite J, Jouhara H, Czajczyńska D, et al. Municipal solid waste management and waste-to-energy in the context of a circular economy and energy recycling in Europe. *Energy*. 2017;141:2013-2044.
2. Chen W-L, Huang C-W, Li Y-H, Kao C-C, Cong HT. Biosyngas-fueled platinum reactor applied in micro combined heat and power system with a thermophotovoltaic array and Stirling engine. *Energy*. 2020;194:116862.
3. Kuo W-C, Lasek J, Słowik K, et al. Low-temperature pretreatment of municipal solid waste for efficient application in combustion systems. *Energ Conver Manage*. 2019;196:525-535.
4. Li Y-H, Chen H-H. Analysis of syngas production rate in empty fruit bunch steam gasification with varying control factors. *Int J Hydrogen Energy*. 2018;43(2):667-675.
5. Li Y-H, Chen G-B, Lin Y-C, Chao Y-C. Effects of flue gas recirculation on the premixed oxy-methane flames in atmospheric condition. *Energy*. 2015;89:845-857.
6. Wang N, Liu S, Liu J. The influence of oxygen concentration on biomass gas micro gas turbine oxygen-enriched combustion. Paper presented at: Proceedings of the 2nd IET Renewable Power Generation Conference (RPG 2013); 2013:1–4.

7. Wall T, Liu Y, Spero C, Elliott L, et al. An overview on oxyfuel coal combustion—state of the art research and technology development. *Chem Eng Res Des*. 2009;87(8):1003-1016.
8. Duan L, Zhao C, Zhou W, Qu C, Chen X. O2/CO2 coal combustion characteristics in a 50kWth circulating fluidized bed. *Int J Greenhouse Gas Control*. 2011;5(4):770-776.
9. Luo SY, Xiao B, Hu ZQ, Liu SM, Guan YW. Experimental study on oxygen-enriched combustion of biomass micro fuel. *Energy*. 2009;34(11):1880-1884.
10. Kayahan U, Özdoğan S. Oxygen enriched combustion and co-combustion of lignites and biomass in a 30 kWth circulating fluidized bed. *Energy*. 2016;116:317-328.
11. Liu L, Huang Y, Cao J, et al. Experimental study of biomass gasification with oxygen-enriched air in fluidized bed gasifier. *Sci Total Env*. 2018;626:423-433.
12. Thornock J, Tovar D, Tree DR, Xue Y, Tsiava R. Radiative intensity, no emissions, and burnout for oxygen enriched biomass combustion. *Proc Combust Inst*. 2015;35(3):2777-2784.
13. Li Y-H, Lin H-T, Xiao K-L, Lasek J. Combustion behavior of coal pellets blended with miscanthus biochar. *Energy*. 2018; 163:180-190.
14. Huang C-W, Li Y-H, Xiao K-L, Lasek J. Cofiring characteristics of coal blended with torrefied miscanthus biochar optimized with three Taguchi indexes. *Energy*. 2019;172:566-579.
15. Corna N, Bertulessi G. The use of oxygen in biomass and waste-to-energy plants: a flexible and effective tool for emission and process control. Paper presented at: Proceedings of the 3rd International Symposium on Energy from Biomass and Waste Venice; 2010.
16. Nunes LJR, Matias JCO, Catalão JPS. Mixed biomass pellets for thermal energy production: a review of combustion models. *Appl Energy*. 2014;127:135-140.
17. Lasek JA, Kopczyński M, Janusz M, Iluk A, Zuwała J. Combustion properties of torrefied biomass obtained from flue gas-enhanced reactor. *Energy*. 2017;119:362-368.
18. Karim MR, Naser J. Numerical modelling of solid biomass combustion: difficulties in initiating the fixed bed combustion. *Energy Proc*. 2017;110:390-395.
19. Fu Z, Zhu J, Barghi S, Zhao Y, Luo Z, Duan C. Minimum fluidization velocity growth due to bed inventory increase in an air dense medium fluidized bed. *Chem Eng J*. 2019;359:1372-1378.
20. Lan W, Chen G, Zhu X, Wang X, Wang X, Xu B. Research on the characteristics of biomass gasification in a fluidized bed. *J Energy Inst*. 2018;92(3):613-620.
21. Scala F, Chirone R, Meloni P, et al. Fluidized bed desulfurization using lime obtained after slow calcination of limestone particles. *Fuel*. 2013;114:99-105.
22. Li P-W, Chyang C-S. A comprehensive study on NOx emission and fuel nitrogen conversion of solid biomass in bubbling fluidized beds under staged combustion. *J Energy Inst*. 2019;93(1) 324-334.
23. Pang L, Shao Y, Zhong W, Liu H. Experimental investigation on the coal combustion in a pressurized fluidized bed. *Energy*. 2018;165:1119-1128.
24. Chirone R, Miccio F, Scala F. On the relevance of axial and transversal fuel segregation during the FB combustion of a biomass. *Energy Fuel*. 2004;18(4):1108-1117.
25. Chirone R, Miccio F, Scala F. Mechanism and prediction of bed agglomeration during fluidized bed combustion of a biomass fuel: effect of the reactor scale. *Chem Eng J*. 2006;123(3):71-80.
26. Saastamoinen J. Release profile of volatiles in fluidised bed combustion of biomass. *J Fundam Renew Energy Appl*. 2015;5: 1-12.
27. Mladenović M, Paprika M, Marinković A. Denitrification techniques for biomass combustion. *Renew Sustain Energy Rev*. 2018;82:3350-3364.
28. Vassilev SV, Baxter D, Andersen LK, Vassileva CG. An overview of the composition and application of biomass ash Part 1. phase–mineral and chemical composition and classification. *Fuel*. 2013;105:40-76.
29. Coats AW, Redfern JP. Thermogravimetric analysis. *A Rev Anal*. 1963;88(1053):906-924.
30. Taguchi G. Introduction to quality engineering: designing quality into products and processes; 1986.
31. Bhatt MS, Mandi RP, Jothibasu S, Rajkumar N. Performance enhancement in coal fired thermal power plants. Part IV: overall system. *Int J Energy Res*. 1999;23(14):1239-1266.
32. Li Y, Yang D, Qu M, Suo L, Sun W. Experimental investigation on co-combustion kinetics and gas emission law of sewage sludge–bituminous coal. *Int J Energy Res*. 2018;42(13):4097-4107.
33. Morgan PA, Robertson SD, Unsworth JF. Combustion studies by thermogravimetric analysis: 1. Coal oxidation. *Fuel*. 1986;65 (11):1546-1551.
34. Lu J-J, Chen W-H. Investigation on the ignition and burnout temperatures of bamboo and sugarcane bagasse by thermogravimetric analysis. *Appl Energy*. 2015;160:49-57.
35. Sun R, Ismail TM, Ren X, El-Salam MA. Effect of ash content on the combustion process of simulated MSW in the fixed bed. *Waste Manag*. 2016;48:236-249.
36. Chen G-L, Chen G-B, Li Y-H, Wu W-T. A study of thermal pyrolysis for castor meal using the Taguchi method. *Energy*. 2014;71:62-70.
37. Karna DS, Scholar AP. An overview on taguchi method; 2019.
38. Basu P. Chapter 10 - biomass cofiring and torrefaction. In: Basu P, ed. *Biomass Gasification, Pyrolysis and Torrefaction*. 2nd ed. Boston, MA: Academic Press; 2013:353-373.
39. Brachi P, Chirone R, Miccio M, Ruoppolo G. Fluidized bed torrefaction of biomass pellets: a comparison between oxidative and inert atmosphere. *Powder Technol*. 2019;357:97-107.
40. Grace JR, Bi H. Introduction to circulating fluidized beds. In: Grace JR, Avidan AA, Knowlton TM, eds. *Circulating Fluidized Beds*. Dordrecht, Netherlands: Springer; 1997:1-20.
41. Wu K-K, Chang Y-C, Chen C-H, Chen Y-D. High-efficiency combustion of natural gas with 21–30% oxygen-enriched air. *Fuel*. 2010;89(9):2455-2462.
42. Huynh CV, Kong S-C. Combustion and NOx emissions of biomass-derived syngas under various gasification conditions utilizing oxygen-enriched-air and steam. *Fuel*. 2013;107: 455-464.

How to cite this article: Li Y-H, Kuo W-C. The study of optimal parameters of oxygen-enriched combustion in fluidized bed with optimal torrefied woody waste. *Int J Energy Res*. 2020;44:7416–7434. https://doi.org/10.1002/er.5459